A MODIFIED GTN MODEL FOR THE PREDICTION OF DUCTILE FRACTURE AT LOW STRESS TRIAXIALITIES

F. Reis[1], L. Malcher[1], F. M. Andrade Pires[1], J. M. A. César de Sá[1]

[1]IDMEC – Institute of Mechanical Engineering
Faculty of Engineering, University of Porto
Rua Dr. Roberto Frias, Porto 4200-465, Portugal
e-mail: fpires@fe.up.pt

ABSTRACT

In this contribution, the so-called GTN constitutive model [1] is extended in order to include a shear mechanism on the damage evolution equation, which depends on the Lode angle. This mechanism is introduced in order to improve the damage prediction under shear dominated loads. From the numerical viewpoint, a fully implicit elastic predictor/return mapping algorithm is developed and the associated consistent elasto-plastic tangent operator is presented. The numerical model is assessed through the simulation of pure shear and combined shear/tensile stress states. Some representative results show the influence of the modifications on the constitutive model of several parameters such as porosity and accumulated plastic strain. A comparative study demonstrates that the proposed model provides better agreement with experimental evidence.

KEY WORDS: GTN model, Low stress triaxiality, Ductile materials, Shear tests, Lode angle dependence.

1. INTRODUCTION

Many classical ductile damage models have the ability to predict the correct fracture location. However, most of them is only effective within a specific range of stress triaxialities. For instance, Lemaitre's model [2] provides good predictions under pure shear or combined shear/tensile stress states, where typically low stress triaxialities are present.

However, at high stress triaxialities, Gurson's original model [3] is more accurate than Lemaitre's. In this case, Gurson's model predicts failure onset for a lower displacement value than Lemaitre's. As reported in a previous contribution [4], this result is in agreement with experimental evidence. This stems from the fact that Gurson's original model is particularly able to capture spherical void growth which is the most relevant mechanism present at high triaxialities. However, under shear dominated stress states, failure mechanisms are driven by shear localization of plastic strain of the inter-voids ligaments due to void rotation and distortion [5]. Since Gurson's original model does not include such important mechanisms, it is not able to capture the behavior of the material under these conditions, yielding on poorer predictions as it will be clear in the following.

In a pure shear test, failure is predicted with reasonable accuracy with Lemaitre's model (see Figure 1). However, this is not the case when Gurson's original model is adopted, since the value of the porosity remains constant once we reach a prescribed displacement and never reaches its critical value. This is a direct consequence of Gurson's constitutive theory that only takes into account the nucleation of micro-voids. Thus, we can conclude that, in order to capture the behavior of a ductile material close to rupture under shear dominated loads, a shear mechanism must also be included.

The evolution laws for internal degradation in Lemaitre

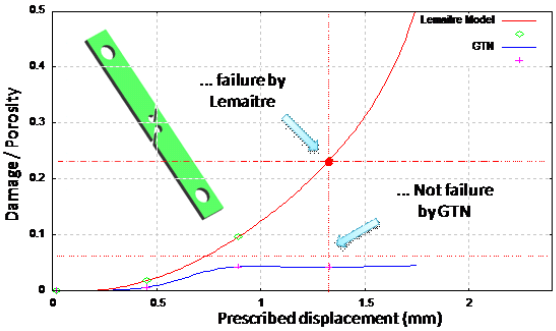

Figure 1. Evolution of the damage and porosity parameters in a pure shear test with Lemaitre's and Gurson's models.

and Gurson material models are dependent on the pressure through the stress triaxiality parameter. Nevertheless, many researchers advocate that damage evolution depends on more than one parameter and that its definition depending solely on the stress triaxiality is not sufficiently accurate (e.g. Brünig et al. [6], Malcher et al. [4], Xue [5], Nahshon and Hutchinson [7]). In this context, several authors (e.g. Brünig et al. [6], Bao and Wierzbicki [8], Xue [5], Nahshon and Hutchinson [7]) have proposed the introduction of the effect of the third invariant of the deviatoric stress tensor through the

so-called *Lode angle* on the set of damage evolution equations.

The goal of this work is to improve the capability of predicting the correct fracture location for a wider range of stress triaxialities. The Lode angle parameter is defined on the deviatoric plane as being the smallest angle between the line of pure shear and the projection of the stress vector on the π-plane. This parameter is responsible for the shape of the yield surface and its effect can be introduced into the constitutive model or into damage evolution law through the so-called Lode angle function.

More recently, Xue [5] has proposed an improvement on the porosity evolution law aiming to capture the behavior of the material at low stress triaxialities through a shear mechanism which is Lode angle dependent. However, although this model has shown significant improvements, its numerical implementation is extremely difficult.

Therefore, this paper has two main goals: (a) to describe the enhancements achieved by the introduction of a shear mechanism into the GTN model which was based inspired in the work of Xue [5]; (b) to suggest a suitable modification of this mechanism aiming to facilitate the numerical implementation and increase efficiency of the constitutive integration algorithm.

2. CONSTITUTIVE MODELING

Gurson's [3] approach has been proposed to describe material internal degradation in the presence of plastic strains. This model, which was developed to provide the "bridge" between material plasticity and damage accumulation, allows the prediction of the loss of resistance of porous materials due to the growth of spherical micro-voids. The main feature of Gurson's model is the introduction of a yield function that is governed by first and second invariant of stress tensor and also by the damage variable f, which represents the volume fraction of micro-voids embedded in the material matrix.

2.1. GTN original model

One of the most commonly employed versions of Gurson's model is the Tvergaard-Needleman modification [1], commonly referred to as GTN model. The model assumes isotropic hardening and isotropic damage (represented by the effective porosity f^*). In the GTN model, the flow potential is generalized into the form:

$$\Phi\left(\underline{\boldsymbol{\sigma}}, k, f\right) = J_2\left(\underline{\boldsymbol{S}}\right) - \frac{1}{3}\left\{1 + q_3.f^{*^2} - 2.q_1.f^*.\cosh\left(\frac{3.q_2.p}{2.\sigma_0}\right)\right\}.\sigma_0^2 \tag{1}$$

where J_2 represents the second invariant of the deviatoric stress tensor, p is the pressure, σ_0 is the isotropic hardening rule (which can be defined as $\sigma_0 = R - \sigma_{y0}$) and R represents the isotropic hardening state variable. The parameters q_1, q_2 and q_3 are introduced to bring the model predictions into closer agreement with full numerical analyses of a periodic array of voids.

The effective porosity reproduces the mechanisms of nucleation, growth and coalescence of voids (which may occur either simultaneously or successively):

$$f^* = \begin{cases} f & , \quad f < f_c \\ f_c + \left(\frac{1}{q_1} - f_c\right)\frac{(f-f_c)}{(f_f-f_c)} & , \quad f \geq f_c \end{cases} \tag{2}$$

where f_c is the value of void volume fraction that defines the beginning of coalescence phenomenon and f_f represents the porosity at fracture. The evolution of f is a sum of the nucleation and growth mechanisms:

$$\dot{f} = \dot{f}^N + \dot{f}^G \tag{3}$$

The nucleation mechanism in this case is driven by the plastic strain:

$$\dot{f}^N = \frac{f_N}{s_N.\sqrt{2\pi}}.\exp\left[-\frac{1}{2}\left(\frac{\overline{\varepsilon}^p - \varepsilon_N}{s_N}\right)^2\right]\dot{\overline{\varepsilon}}^p \tag{4}$$

where f_N represents the volume fraction of all second-phase particles with potential for micro-void nucleation, ε_N and s_N are the mean strain for void nucleation and its standard deviation. The variable $\overline{\varepsilon}^p$ represents the equivalent plastic strain and $\dot{\overline{\varepsilon}}^p$ is the rate of the accumulated plastic strain.

The most significant contribution is the growth of existing voids, denoted by $\dot{f}^G$, obtained from the condition of plastic incompressibility of the matrix material:

$$\dot{f}^G = (1-f).tr\left(\dot{\boldsymbol{\varepsilon}}^p\right) = (1-f).\dot{\varepsilon}_v^p \tag{5}$$

where $\dot{\varepsilon}_v^p$ represents the rate of the volumetric plastic strain.

2.2. Shear mechanism

In order to improve the GTN model ability to capture the behavior of ductile materials close to rupture at low stress triaxialities, Xue [5] has proposed the inclusion of a shear mechanism which is a function of the porosity, equivalent strain and the Lode angle. Originally, the shear mechanism was developed considering geometrical considerations in a cell structure with a circular void at the center subjected to a simple shear strain (for more details, see Xue [5]). After some straightforward algebra manipulation, the rate of this mechanism is expressed as:

$$\dot{f}^{Shear} = q_4.f^{q_5}.g_0.\varepsilon_{eq}.\dot{\varepsilon}_{eq} \tag{6}$$

where q_4 and q_5 are parameters related to two- or three-dimensional problems, respectively set to $q_4 = 1.69$ and

$q_5 = 1/2$, $q_4 = 1.86$ and $q_5 = 1/3$. The parameter f represents the porosity, ε_{eq} is the equivalent strain and g_0 is a parameter responsible to incorporate the Lode angle dependence in the shear mechanism and that can be defined as:

$$g_0 = 1 - \frac{6.\|\theta\|}{\pi} \tag{7}$$

where θ is the Lode or azimuth angle, which can be determined as:

$$\theta = tan^{-1}\left\{\frac{1}{\sqrt{3}}\left[2.\left(\frac{S_2 - S_3}{S_1 - S_3}\right) - 1\right]\right\} \tag{8}$$

in which S_1, S_2 and S_3 are components of the deviatoric stress tensor in the principal plane.

The shear mechanism proposed by Xue can be added to the GTN model which already features the mechanisms of nucleation and growth of micro-voids. Thus, the evolution of the porosity now reads:

$$\dot{f} = \dot{f}^N + \dot{f}^G + \dot{f}^{Shear} \tag{9}$$

2.3. The proposed modification

The shear mechanism was suggested in order to introduce void elongation effect into the original GTN model. Therefore, the contribution of such mechanism is higher at low stress triaxialities and, through the definition of the parameter g_0, for low values of the Lode angle. In this contribution, the evolution of the porosity due to shear effects will be a function of both the accumulated plastic strain and the rate of the accumulated plastic strains instead of the total strain and total strain rate. This simplification is resoanable in the majority of problems since the elastic strains can be considered negligible.

$$\dot{f}^{Shear} = q_4.f^{q_5}.g_0.\overline{\varepsilon}^p.\dot{\overline{\varepsilon}}^p \tag{10}$$

The Lode angle function can also be rewritten as a function of the normalized third invariant:

$$g_0 = 1 - \left\|\overline{\theta}\right\| \tag{11}$$

where $\overline{\theta}$ represents the normalized Lode angle which is a function of the normalized third invariant [8]:

$$\overline{\theta} = 1 - \frac{6.\theta}{\pi} = 1 - \frac{2}{\pi}\arccos\xi \tag{12}$$

In the equation above, ξ represents the normalized third invariant and can be calculated as:

$$\xi = \frac{27}{2}\frac{det\left(\boldsymbol{\varepsilon}_d^e\right)}{\left(\frac{3}{2}\boldsymbol{\varepsilon}_d^e : \boldsymbol{\varepsilon}_d^e\right)^{\frac{3}{2}}} \tag{13}$$

where $\boldsymbol{\varepsilon}_d^e$ represents the deviatoric elastic strain tensor [9]. The initial value of the normalized Lode angle for different stress conditions is represented in Figure 2 [9]. As we can see in Figure 2, in pure shear conditions, $\bar{\theta}$ is around zero which correspond a value of g_0 around 1.

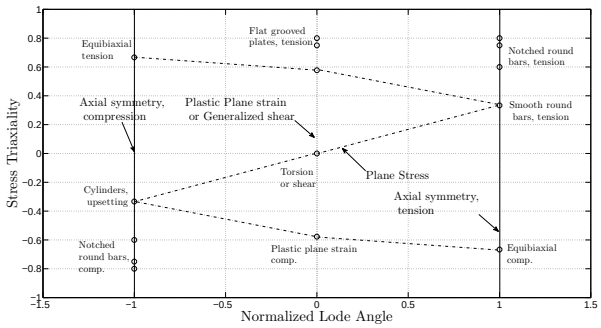

Figure 2. Triaxiality as a function of the Normalized Lode angle for initial stress states [9].

In this case, the effect of the shear mechanism is added to the damage variable of the original GTN model. On the other hand, in traction problems with round bars, the Lode angle function is approximately zero and in these cases, the shear mechanism proposed does not play any role.

2.4. Integration algorithm

As already pointed out, the proposed modification leads us to a constitutive model which is easier to implement than the model proposed by Xue. The constitutive equations of the model are integrated implicitly by using a typical elastic predictor/return mapping algorithm (a detailed discussion on return mapping algorithms can be found elsewhere, e.g., Simo and Hughes [10], de Sousa Neto et al. [11], etc.). Straightforward (pseudo-)time discretization of the constitutive equations leads to the following system of equations:

$$\begin{cases} r_{\Delta\gamma} = \frac{1}{2}\frac{\boldsymbol{s}^{Trial} : \boldsymbol{s}^{Trial}}{1 + 2.G.\Delta\gamma^2} \\ \qquad - \frac{1}{3}\left\{1 + q_3.f_{n+1}^2 - 2.q_1.f_{n+1}.\cosh\left(\frac{3.q_2.p_{n+1}}{2.\sigma_0}\right)\right\}.\sigma_0^2 \\ r_p = p_{n+1} - p_{n+1}^{Trial} + \Delta\gamma.K.q_1.q_2.f_{n+1}.\sigma_0.\sinh\left(\frac{3.q_2.p_{n+1}}{2.\sigma_0}\right) \\ r_f = fn + 1 - f_{n+1}^{Trial} - \Delta f^G - \Delta f^{Trial} \\ r_R = R_{n+1} - R_{n+1}^{Trial} - \Delta R_{n+1} \end{cases} \tag{14}$$

which needs to be solved for $\Delta\gamma$, p_{n+1}, f_{n+1} and R_{n+1}. Here, we choose to apply the standard Newton-Raphson method for the solution of the non-linear system. The residual system of equations, on the linearized form can be given by:

$$\begin{bmatrix} \frac{\partial r_{\Delta\gamma}}{\partial\Delta\gamma} & \frac{\partial r_{\Delta\gamma}}{\partial p_{n+1}} & \frac{\partial r_{\Delta\gamma}}{\partial f_{n+1}} & \frac{\partial r_{\Delta\gamma}}{\partial R_{n+1}} \\ \frac{\partial r_p}{\partial\Delta\gamma} & \frac{\partial r_p}{\partial p_{n+1}} & \frac{\partial r_p}{\partial f_{n+1}} & \frac{\partial r_p}{\partial R_{n+1}} \\ \frac{\partial r_f}{\partial\Delta\gamma} & \frac{\partial r_f}{\partial p_{n+1}} & \frac{\partial r_f}{\partial f_{n+1}} & \frac{\partial r_f}{\partial R_{n+1}} \\ \frac{\partial r_R}{\partial\Delta\gamma} & \frac{\partial r_R}{\partial p_{n+1}} & \frac{\partial r_R}{\partial f_{n+1}} & \frac{\partial r_R}{\partial R_{n+1}} \end{bmatrix}^k \cdot \begin{bmatrix} \delta\Delta\gamma \\ \delta p_{n+1} \\ \delta f_{n+1} \\ \delta R_{n+1} \end{bmatrix}^{k+1} = -\begin{bmatrix} r_{\Delta\gamma}\left(\Delta\gamma, p, f, R\right) \\ r_p\left(\Delta\gamma, p, f, R\right) \\ r_f\left(\Delta\gamma, p, f, R\right) \\ r_R\left(\Delta\gamma, p, f, R\right) \end{bmatrix}^k \tag{15}$$

where we need to determine the derivatives of $r_{\Delta\gamma}$, r_p and r_R in respect to every unknown of the problem.

The associated consistent elastoplastic tangent operator, necessary to ensure quadratic convergence rates, can be expressed in the following closed-form:

$$\begin{aligned}\boldsymbol{D^{ep}} = & \frac{2.G}{(1+2.G.\Delta\gamma)}\left(\mathsf{I} - \frac{1}{3}\boldsymbol{I}\otimes\boldsymbol{I}\right) \\ & + \left[\frac{2.G}{(1+2.G.\Delta\gamma)}\right]^2 .\boldsymbol{\varepsilon}^{e\ trial}_{d\ n+1} \\ & \otimes\left[\left(C_{11}\frac{\partial r_{\Delta\gamma}}{\partial \boldsymbol{\varepsilon}^{e\ Trial}_{d\ n+1}} + C_{13}\frac{\partial r_f}{\partial \boldsymbol{\varepsilon}^{e\ Trial}_{d\ n+1}}\right) C_{12}\frac{\partial r_p}{\partial \varepsilon^{e\ Trial}_{v\ n+1}}\boldsymbol{I}\right] \\ & - \boldsymbol{I}\otimes\left[\left(C_{21}\frac{\partial r_{\Delta\gamma}}{\partial \boldsymbol{\varepsilon}^{e\ Trial}_{d\ n+1}} + C_{23}\frac{\partial r_f}{\partial \boldsymbol{\varepsilon}^{e\ Trial}_{d\ n+1}}\right) + C_{22}\frac{\partial r_p}{\partial \varepsilon^{e\ Trial}_{v\ n+1}}\boldsymbol{I}\right]\end{aligned} \tag{16}$$

where C_{11}, C_{12}, C_{21}, C_{23} and C_{22} are constants associated with the non-linear system. Furthermore, I and I are respectively the fourth and second order identity tensors.

3. NUMERICAL RESULTS

In this section, the performance of the extended constitutive model is assessed by means of two examples. Both were simulated considering a finite strain formulation in an in-house finite element code.

3.1. Shear test

To illustrate the effectiveness of the proposed constitutive model, a shear specimen subject to a shear stress state has been analysed [6].

A three-dimensional finite element mesh with 8-node linear elements with *FBAR* technology (for more details see [11]) has been employed in all analyses (see Figure 3). The material properties adopted are listed in Table 1.

Table 1. Material properties for the aluminum alloy (Al 2024-T351).

Description	Symbol	Value
Density	ρ	$2.7\times10^3\ kg/m^3$
Elastic modulus	E	$7.115\times10^4\ [MPa]$
Poisson's ratio	v	0.3
Initial yield stress	σy_0	$370\ [MPa]$
Hardening curve	$\sigma_y\ (\overline{\varepsilon}^p)$	$908\ (0.0058+\overline{\varepsilon}^p)^{0.1742}$ $[MPa]$
q_1		1.5
q_2		1
q_3		2.25
Volumetric fraction of micro-void for nucleation for nucleation	f_N	0.04
Mean strain of void nucleation	ε_N	0.2
Standard deviation strain for nucleation	S_N	0.1

Figure 4.a shows the evolution of porosity for the two Gurson based models. In this test, where the triaxiality ratio attains a value around zero, we can observe that the modified GTN model proposed herein has the ability of predicting the degradation associated

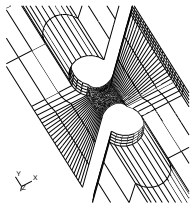

Figure 3. Finite element mesh for the shear specimen with 3432 elements and 4785 nodes.

with shear effects. The original GTN model, however, provides an inaccurate response when the shear effects are present. This can be concluded since porosity remains constant when the prescribed displacement is increased. Thus, the proposed model has the ability to predict shear effects as well as nucleation and growth of micro-voids. Even though the final values of the damage variable are considerable distinct, when we compare the distributions of damage in the shear specimen we conclude that the distribution is similar (see Figure 5).

In Figure 4.b, the evolution of accumulated plastic strain is plotted. As expected, this internal variable is larger when the new model is considered since degradation is significantly higher if compared with GTN original model that only contemplates nucleation and growth mechanisms. In contrast with the accumulated plastic strain, we can see in Figure 4.c that the reaction force associated with the new model is smaller than the similar curve associated with GTN model. Again, this difference is a consequence of an higher internal damage. One interesting aspect to note in Figure 4.c is the pronounced effect of softening in the reaction curve of the new model for the same prescribed displacement.

Moreover, the efficiency of the proposed algorithm is also assessed. Table 2 shows a typical residual convergence observed during the analysis of the present example. Clearly, convergence exhibits a quadratic convergence rate due to the consistent tangent operator.

Table 2. Typical global convergence of proposed model.

Iteration	Relative residual norm (%)
1	4.57572
2	0.559380E-01
3	0.978862E-05
4	0.495718E-09

3.2. Flat-grooved test

In this section, a flat-grooved plate [12] in plane strain is analysed under a tensile dominant load. The main goal of the numerical simulation is to verify the ability of the

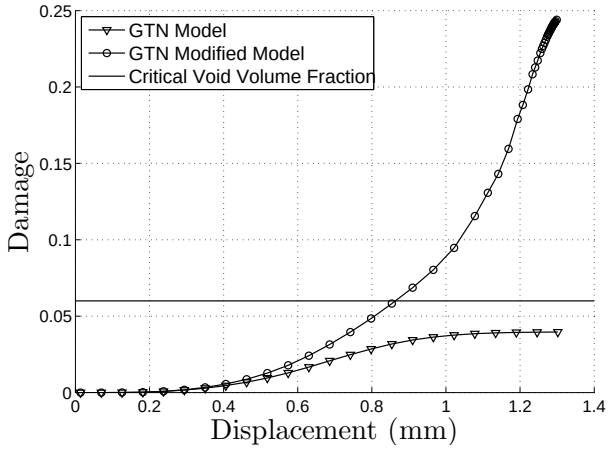

a)

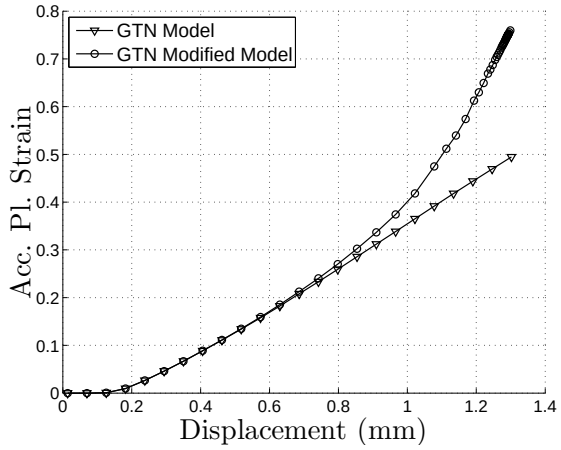

b)

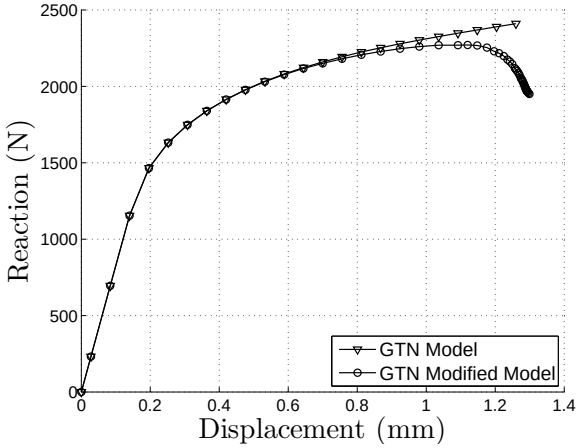

c)

Figure 4. (a) Evolution of damage; (b) evolution of accumulated plastic strain; (c) reaction curve

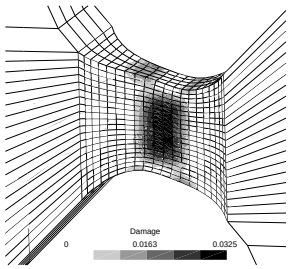

a)

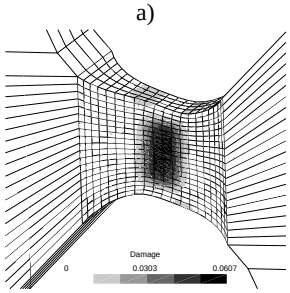

b)

Figure 5. Distribution of damage a) GTN model; b) New model.

proposed model to predict the 45 degrees inclined shear bands observed in experimental testing [5]. The material properties are the same as the material in the preceding section (see Table 1). Spatial discretization has been done by using 8-node quadratic elements with a reduced integration scheme (see Figure 6).

Figure 6. Finite element mesh for the plane strain specimen with 1600 elements and 5033 nodes.

In Figure 6, we can clearly observe the effects of the incorporated shear mechanism. For the same applied displacement, the contours of the new damage variable have correctly predicted the shear bands inclined 45 degrees in respect to the loading direction. In the simulation with the original GTN model, however, damage has concentrated at the center of the specimen which is not in agreement with experimental results [5].

4. CONCLUSIONS

In this work, we have briefly revised the original GTN model and depicted its limitations when subject to low triaxialities. For such model, the damage variable (volume fraction of voids dependent on pressure) does not reflect the degradation associated with shear effects. The incorporation of a modified shear mechanism into the constitu-

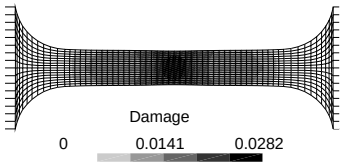

(a)

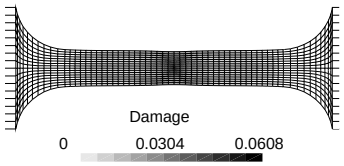

(b)

Figure 7. Damage contours at critical zone for the plane strain test: (a) original GTN model; (b) proposed model.

tive model has allowed a much more accurate prediction of failure for a wider range of triaxialities. Finally, the modified evolution of the porosity due to shear effects proposed in this paper has provided an extremely efficient numerical implementation exhibiting high asymptotic convergence rates.

ACKNOWLEDGEMENTS

Fábio Reis is supported by Portuguese Science and Technology Foundation (FCT), under scholarship number SFRH/BD/60887/2009. Lucival Malcher is supported by Portuguese Science and Technology Foundation (FCT), under scholarship number SFRH/BD/45456/2008. The authors acknowledge the support of Portuguese Science and Technology Foundation (FCT) under grant with reference PTDC/EME-TME/71325/2006.

REFERENCES

[1] V Tvergaard and A. Needleman. Analysis of cup-cone fracture in a round tensile bar. *Acta Metallurgica*, 32:157–169, 1984.

[2] J. Lemaitre. *A Course on Damage Mechanics*. Springer, 1990.

[3] A.L. Gurson. Continuum theory of ductile rupture by void nucleation and growth - part I: Yield criteria and flow rule for porous media. *Journal of Engineering Materials and Technology*, 99:2–15, 1977.

[4] L. Malcher, F. M. Andrade Pires, J. M. A. César de Sá, and F. X. C. Andrade. Comparative study between ductile damage constitutive model. In *COMPLAS*, Spain, Barcelona, 2009.

[5] L. Xue. *Ductile Fracture Modeling - Theory, Experimental Investigation and Numeriacl Verification*. PhD thesis, Massachusetts Institute Technology, 2007.

[6] M. Brünig, O. Chyra, D. Albrecht, L. Driemeier, and M. Alves. A ductile damage criterion at various stress triaxialities. *International Journal of Plasticity*, 24:1731–1755, 2008.

[7] L. Nahshon and J. W. Hutchinson. Modification of the gurson model for shear failure. *European Journal of Mechanics A/Solids*, 27:1–17, 2008.

[8] Y. Bao and T. Wierzbicki. On fracture locus in the equivalent strain and stress triaxiality space. *International Journal of Mechanical Sciences*, 46(81): 81–98, 2004.

[9] Y. Bai. *Effect of Loading History on Necking and Fracture*. PhD thesis, Massachusetts Institute Technology, 2008.

[10] J. C. Simo and T. J. R Hughes. *Computational Inelasticity*. Springer, 1998.

[11] E. A. de Sousa Neto, D. Perić, and D. R. Owen. *Computational Methods for Plasticity: Theory and Application*. Wiley, 2008.

[12] X. Teng. Numerical prediction of slatn fracture with continuum damage mechanics. *Engineering Fracture Mechanics*, 75:2020–2041, 2008.